

Proteome-Wide Characterization of the RNA-Binding Protein RALY-Interactome Using the *in Vivo*-Biotinylation-Pulldown-Quant (iBioPQ) Approach

Stefan Tenzer,^{#,†} Albertomaria Moro,^{#,‡} Jörg Kuharev,[†] Ashwanth Christopher Francis,[§] Laura Vidalino,[‡] Alessandro Provenzani,[¶] and Paolo Macchi^{*,‡}

[†]Institute for Immunology, University Medical Center of the Johannes Gutenberg-University Mainz, Langenbeckstrasse 1, 55131 Mainz, Germany

[‡]Laboratory of Molecular and Cellular Neurobiology, CIBIO-Centre for Integrative Biology, University of Trento, via Delle Regole 101, 38060, Mattarello, Trento, Italy

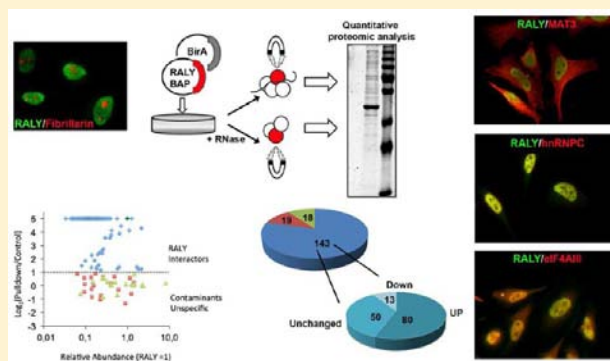
[§]Laboratory of Molecular Virology, CIBIO-Centre for Integrative Biology, University of Trento, Trento, Italy

[¶]Laboratory of Genomic Screening, Centre for Integrative Biology, University of Trento, Trento, Italy

S Supporting Information

ABSTRACT: RALY is a member of the heterogeneous nuclear ribonucleoproteins, a family of RNA-binding proteins generally involved in many processes of mRNA metabolism. No quantitative proteomic analysis of RALY-containing ribonucleoproteins (RNPs) has been performed so far, and the biological role of RALY remains elusive. Here, we present a workflow for the characterization of RALY's interaction partners, termed iBioPQ, that involves *in vivo* biotinylation of biotin acceptor peptide (BAP)-fused protein in the presence of the prokaryotic biotin holoenzyme synthetase of BirA so that it can be purified using streptavidin-coated magnetic beads, circumventing the need for specific antibodies and providing efficient pulldowns. Protein eluates were subjected to tryptic digestion and identified using data-independent acquisition on an ion-mobility enabled high-resolution nanoUPLC-QTOF system. Using label-free quantification, we identified 143 proteins displaying at least 2-fold difference in pulldown compared to controls. Gene Ontology overrepresentation analysis revealed an enrichment of proteins involved in mRNA metabolism and translational control. Among the most abundant interacting proteins, we confirmed RNA-dependent interactions of RALY with MATR3, PABP1 and ELAVL1. Comparative analysis of pulldowns after RNase treatment revealed a protein–protein interaction of RALY with eIF4AIII, FMRP, and hnRNP-C. Our data show that RALY-containing RNPs are much more heterogeneous than previously hypothesized.

KEYWORDS: proteomics, biotinylation, protein–protein interactions RALY, heterogeneous nuclear ribonucleoproteins, RNA-binding proteins



INTRODUCTION

The heterogeneous nuclear ribonucleoproteins (hnRNPs) is a family consisting of more than 20 RNA-binding proteins, which exert several roles in the RNA metabolism, such as splicing, mRNA stability and nuclear export in many different cell types.^{1–5} Some hnRNPs are also known to recruit regulatory proteins associated with molecular pathways related to DNA metabolism and DNA damage repair.⁶ Although the hnRNPs are the most abundant nuclear proteins, some of them shuttle between the nucleus and the cytoplasm where they can remain associated to the cognate mRNA during its transport, subcellular localization and subsequent translation.^{7–11} Generally, hnRNPs are characterized by the presence of one or two

RNA-binding motifs (RRMs), whose consensus sequence can vary among the members of the family.^{3,12}

RALY, also known as hnRNP C-related protein, is a member of the hnRNP family that was initially identified as an autoantigen cross-reacting with the Epstein–Barr nuclear antigen 1 (EBNA1), a viral protein associated with Epstein–Barr virus.¹³ Subsequent studies associated a genomic deletion of Raly with the lethal yellow mutation, being the *Raly* gene locus near to the locus *A^y* in this mouse.^{14,15} In human colon adenocarcinoma cell line, RALY together with NONO/p54nrb¹⁶ have been identified as interactors of YB-1, an

Received: March 4, 2013

Published: April 24, 2013

RNA-binding protein that is involved in splicing, transcription and translational regulation of specific mRNAs.¹⁷ Importantly, YB-1 overexpression in different tumors has been related with the secondary acquired resistance to specific drugs.^{18,19} Interestingly, RALY transcript is overexpressed in different cancer tissues, and this correlates with a poor outcome of the disease.¹⁷ Depletion of RALY expression by RNAi sensitizes colorectal cancer cell lines treated with the platinum analogue oxaliplatin without affecting the cell growth rate,¹⁷ indicating a potential role of RALY in tumorigenesis that still requires further investigations and mechanistic analysis. RALY was previously identified in spliceosomal complexes, suggesting its possible involvement in RNA splicing.²⁰ RALY and other RNA-binding proteins, including members of the hnRNPs such as hnRNPH/F, were also found in the immunoprecipitates for RBFOX1/2.²¹ RBFOX1/2 are members of a protein family that regulates alternative splicing in a tissue-specific manner.^{22,23} Nevertheless, in contrast to hnRNPH that modulates the splicing activity of RBFOX1/2, RALY has no effects in this process and its misregulation does not impair alternative splicing of RBFOX1/2 mRNA targets.²¹ Although there is evidence that RALY might have multiple roles in RNA metabolism, RALY remains poorly characterized in mammals and the list of its potential protein interactors is still elusive. Because of the difficulty to obtain efficient immunoprecipitating antibodies, the molecular composition of RALY-containing ribonucleoprotein (RNP) complexes is still unknown.

In recent years, mass spectrometric analysis has become the method of choice for the identification of protein interaction partners from affinity purified material.²⁴ Latest developments in mass spectrometry instrumentation facilitate the identification of higher numbers of proteins from limited amounts of sample.²⁵ However, while this enables the identification of not only core interacting proteins but also weaker interaction partners, increasing numbers of contaminating or nonspecifically binding proteins are being identified. This sometimes obscures the interpretation of identified potential interactors and their biological functions.²⁶ To reduce the problem of unspecific binding, highly specific affinity purification methods, including tandem affinity purification, have been developed (for excellent reviews, see refs 27 and 28) to isolate target proteins and their associated binding partners. In the past years, several methods have been described for linking quantitative affinity purification methods to mass spectrometric identification (q-AP-MS) based on SILAC²⁶ or label-free approaches,²⁹ enabling not only the identification, but also the relative quantification of proteins in pulldowns and controls, to identify unspecifically binding proteins. *In vivo* biotinylation-based pulldown has been initially developed to identify site-specific protein modifications³⁰ and the single-step purification of transcription factors.³¹ Furthermore, the same approach has been recently applied to elucidate the FoxP3 interactome, identifying 361 FoxP3 interacting proteins,³² underlining its potential to identify protein interaction partners. However, this technique has not yet been integrated into a label-free quantitative proteomics workflow.

In this study, we applied the iBioPQ approach to identify RALY-associated proteins to learn about the molecular mechanisms underlying the cellular function of RALY. By combining efficient streptavidin-based pulldown of *in vivo* biotinylated RALY with subsequent ion-mobility enhanced, data-independent-acquisition-based label-free quantitative proteomic analysis of pulldowns, we identified 143 protein

components of RALY protein complexes that were either exclusively detected in pulldowns or >2-fold enriched compared to controls. Among these, MATR3, PABP1 and ELAVL1, proteins involved in mRNA metabolism and translational control, were among the most abundant interacting proteins. Moreover, we found that eIF4AIII, FMRP, and hnRNP-C associate with RALY via protein-protein interactions. Our data show that RALY-containing RNPs are much more heterogeneous than previously thought and that RALY might have pleiotropic effects on RNA metabolism and translation.

MATERIALS AND METHODS

Cell Cultures and Expression Constructs

293T and HeLa cells were grown in DMEM supplemented with 10% FCS, at 37 °C and 5% CO₂ atmosphere. Cell lines were transfected using the TransIT transfection reagent (Mirus, Bio LLC) according to the manufacturer's protocol. RT-PCR was performed on total RNA isolated from cells using the TRIzol reagent (Invitrogen). Human RALY cDNA was amplified with the Phusion High-Fidelity DNA polymerase (New England BioLabs) and then cloned in the pEGFP-N1 vector (Clontech). BAP-tagged Raly was created using two complementary primers: 5'-ccgggtggcctgaacgacatcttcaggctcagaaaatcgaatggcagcaataa and 5'-ggccttattcgtccattcgatttctgagcctcgaagatgtcgttcaggccacc. The underlined sequence encodes the BAP peptide (GLNDIFEAQKIEWHE).³⁰ The primers were annealed and cloned in frame to RALY cDNA in the pEGFP-N1 vector lacking the EGFP-coding sequence. The construct to express RALY lacking the glycine-rich region (RALY-ΔGRR) was created using the site-directed mutagenesis kit (Finnzymes, Thermo Scientific) according to the manufacturer's protocol with the following primers: 5'-gagaacacaactctgaggcaggc and 5'-ctgctcaagcggctcagcaggc.

Pulldown Assay

The purification of RALY-BAP was performed using streptavidin-conjugated beads (Invitrogen). Briefly, 293T cells grown on 10 cm Petri dishes were transfected with RALY-BAP and Bir(A) constructs. After 30 h the cells were lysed with NEHN lysis buffer [20 mM HEPES pH 7.5, 300 mM NaCl, 0.5% NP-40, 20% glycerol, 1 mM EDTA, phosphatase and protease inhibitors (Roche)] and incubated for 30 min in ice. 40 μL of beads were then added to 1 mg of protein extract and incubated overnight at 4 °C under rotation. The beads were washed five times with NEHN buffer and incubated for 20 min at room temperature in 40 μL of elution buffer [7 M urea, 2 M thiourea, 2% CHAPS, 20 mM Tris-HCl pH 8]. For RNase treatment, cell extracts were treated either with RNase A (100 μg/mL) for 15 min or with DNase (10 U) for 30 min at 37 °C, before the incubation with beads. For Western blot analysis, 10 μL of purified samples were separated by 12% SDS-PAGE and blotted onto nitrocellulose (Schleicher & Schuell) as previously described.³³ The following primary antibodies were used: rabbit polyclonal anti-PABPC, rabbit polyclonal anti-FMRP, rabbit polyclonal anti-eIF4AIII and mouse monoclonal anti-ELAVL1 (all provided by Abcam); rabbit polyclonal anti-hnRNP-C (Millipore); rabbit polyclonal anti-Matrin3 and rabbit polyclonal anti-PRP19 (GeneTex); anti-YB1 (Santa Cruz); mouse monoclonal anti-Mago and mouse monoclonal anti-Histone H1FX (Abnova); rabbit polyclonal anti-RL7a and rabbit polyclonal anti-beta Tubulin (Cell Signaling); rabbit polyclonal anti-APP (Sigma). The following secondary antibodies were

used: horse radish peroxidase (HRP)-conjugated goat anti-mouse and anti-rabbit antibodies (1:5,000, Santa Cruz Biotechnology). To identify biotinylated RALY-BAP, the membrane was decorated with the rabbit polyclonal anti-RALY antibody (1:5,000; Bethyl). The membrane was then stripped and incubated for 45 min with an HRP-conjugated anti-streptavidin (1:10,000; Pierce). All Western blots were analyzed with the ChemiDoc XRS+ System (Bio-Rad).

Immunocytochemistry and Fluorescence Microscopy

Cells grown on coverslips were washed in prewarmed 1xPBS and then fixed in 4% PFA for 15 min at room temperature. Immunocytochemistry was carried out as previously described³³ using the primary antibodies listed above. To detect RALY-biotinylated, cells were incubated with Alexa-488 labeled avidin (Invitrogen) for 1 h. Alexa 594- and Alexa 488-coupled goat anti-mouse and anti-rabbit IgG antibodies (Molecular Probes) were used as secondary antibodies. Microscopy analysis was performed using the Zeiss Observer Z.1 microscope implemented with the Zeiss ApoTome device. Pictures were acquired using AxioVision imaging software package (Zeiss) and assembled with Adobe Photoshop CS3. Images were not modified other than adjustments of levels, brightness and magnification.

Protein Digestion

Two biological replicates of pulldown and control samples were prepared and processed for LC-MS analysis in parallel. All samples were then analyzed in triplicate by nanoUPLC. Proteins were digested using a modified FASP method.³⁴ Briefly, eluted protein was loaded on the filter, and detergents were removed by washing three times with buffer containing 8 M urea. The proteins were then reduced using DTT and alkylated using iodoacetamide. The excess reagent was quenched by addition of DTT and washed through the filters. Buffer was exchanged by washing with 50 mM NH_4HCO_3 and proteins digested overnight by trypsin (Trypsin Gold, Promega) in with an enzyme to protein ratio of 1:50. After overnight digestion, peptides were recovered by centrifugation and two additional washes using 50 mM NH_4HCO_3 . Flowthroughs were combined, lyophilized and redissolved in 20 μL 0.1% formic acid by sonication. The resulting tryptic digest solutions were diluted with aqueous 0.1% v/v formic acid to a concentration of 200 ng/ μL and spiked with 25 fmol/ μL of enolase 1 (*Saccharomyces cerevisiae*) tryptic digest standard (Waters Corporation).

UPLC-MS Configuration

Nanoscale LC separation of tryptic peptides was performed with a nanoAcquity system (Waters Corporation) equipped with a BEH C18 1.7 μm , 75 μm \times 150 mm analytical reversed-phase column (Waters Corporation) in direct injection mode as described before.³⁵ 0.2 μL of sample (40 ng of total protein) was injected per technical replicate. Mobile phase A was water containing 0.1% v/v formic acid, while mobile phase B was ACN containing 0.1% v/v formic acid. Peptides were separated with a gradient of 3–40% mobile phase B over 120 min at a flow rate of 300 nL/minute, followed by a 10-min column rinse with 90% of mobile phase B. The columns were re-equilibrated at initial conditions for 15 min. The analytical column temperature was maintained at 55 °C. The lock mass compound, [Glu¹]-Fibrinopeptide B (100 fmol/ μL), was delivered by the auxiliary pump of the LC system at 300 nL/

minute to the reference sprayer of the NanoLockSpray source of the mass spectrometer.

Mass spectrometric analysis of tryptic peptides was performed using a Synapt G2-S mass spectrometer (Waters Corporation, Manchester, U.K.). For all measurements, the mass spectrometer was operated in v-mode with a typical resolution of at least 25 000 fwhm (full width half-maximum). All analyses were performed in positive mode ESI. The time-of-flight analyzer of the mass spectrometer was externally calibrated with a NaI mixture from m/z 50 to 1990. The data were postacquisition lock mass corrected using the doubly charged monoisotopic ion of [Glu¹]-Fibrinopeptide B. The reference sprayer was sampled with a frequency of 30 s. Accurate mass LC-MS data were collected in data-independent modes of analysis^{36,37} in combination with online ion mobility separations.³⁸ For ion mobility separation, a wave height of 40 V was applied. Traveling wave velocity was ramped from 800 to 500 m/s over the full IMS cycle. The spectral acquisition time in each mode was 0.7 s with a 0.05-s interscan delay. In low energy MS mode, data were collected at constant collision energy of 4 eV. In elevated energy MS mode, the collision energy was ramped from 25 to 55 eV during each 0.7-s integration. One cycle of low and elevated energy data was acquired every 1.5 s. The radio frequency (RF) amplitude applied to the quadrupole mass analyzer was adjusted such that ions from m/z 350 to 2000 were efficiently transmitted, ensuring that any ions observed in the LC-MS data less than m/z 350 were known to arise from dissociations in the collision cell. All samples were analyzed in triplicate.

Data Processing and Protein Identification

Continuum LC-MS data were processed and searched using ProteinLynx GlobalSERVER version 2.5.2 (Waters Corporation). The resulting peptide and protein identifications were evaluated by the software using statistical models as described.³⁶ Protein identifications were assigned by searching the human taxon of the UniProtKB/SwissProt database (release 2012_01) supplemented with known possible contaminants and standard proteins (porcine trypsin, yeast enolase, BirA, streptavidin) using the precursor and fragmentation data afforded by the LC-MS acquisition method as reported.³⁶ The search parameter values for each precursor and associated fragment ions were automatically set by the software using the measured mass error obtained from processing the raw continuum data. Peptide identifications were restricted to tryptic peptides with no more than one missed cleavage. Carbamidomethyl cysteine was set as fixed modification, and oxidized methionine, protein N-acetylation, and deamidation of asparagine and glutamine were searched as variable modifications. Database search was performed allowing a maximal mass deviation of 3 ppm for precursor ions and 10 ppm for fragment ions. For a valid protein identification, the following criteria had to be met: at least 2 peptides were detected with together at least 7 fragments. All reported peptide identifications provided by the IDENTITY^E-algorithm are correct with >95% probability as described.³⁶ The initial false positive rate for protein identification was set to 3% on the basis of a search of a 5 \times randomized database, which was generated automatically using PLGS2.5.2 by randomizing the sequence of each entry. By using replication rate of identification as a filter, the false positive rate is further reduced to <0.1%. Additional data processing including retention time alignment, normalization, isoform/homology and replicate filtering, as well as final TOP3-

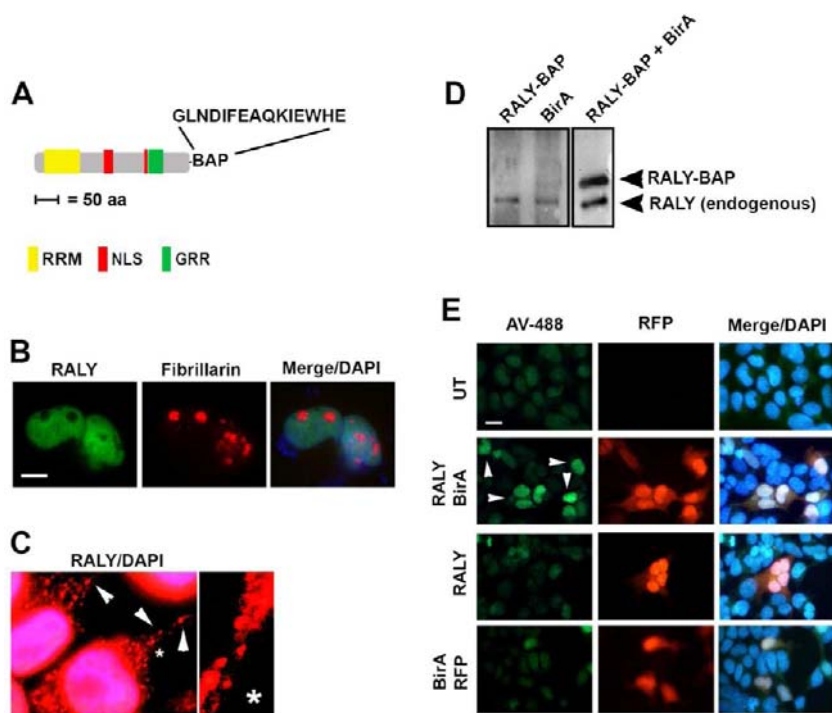


Figure 1. (A) Domain structure of human RALY (accession UniProt: Q9UKM9). Predicted domains are indicated by different colors. The RNA-recognition domain (RRM, amino acids 20–89) and a glycine rich region (GRR, amino acids 227–251) are present at the N- and C-terminal region, respectively. Moreover, two putative NLS (in red, amino acids 145–158 and 218–224, respectively) are predicted. The 15-amino acids sequence of the biotin acceptor peptide (BirA) added to the C-terminal region of RALY is indicated. See also Figure S1A (Supporting Information) for the detailed sequence. (B) Intracellular localization of RALY protein in 293T cells. Dual visualization of endogenous RALY (green) and the nucleolar marker fibrillarin (red). RALY localizes in the nuclei but not in the nucleoli. The nuclei are stained with DAPI. Scale bar = 5 μ m. (C) RALY is detected in the cytoplasm. 293T cells were fixed and stained with a polyclonal antibody anti-RALY. Discrete RALY particles, indicated by arrowheads, are distributed throughout the cytoplasm and at the periphery of the cell. Inset: enlarged view of the area indicated by the asterisk. (D) In vivo biotinylation of RALY. Lysates of transfected 293T cells were prepared as described in Materials and Methods, and the Western blot was decorated with an anti-RALY antibody together with an antistreptavidin antibody that recognizes the biotinylated form of RALY. Biotinylation leads to the shift of RALY-BAP that migrates at a higher molecular weight. In contrast, only the endogenous RALY at 37 kDa is detected in 293T cells transfected with only RALY-BAP or BirA alone, indicating that endogenous biotinylation does not occur in the absence of BirA and RALY-BAP coexpression. Biotinylation of RALY can be detected by a HRP-conjugated antistreptavidin. (E) Intracellular localization of biotinylated RALY. Biotinylated RALY shows a remarkably similar localization with endogenous RALY in the nucleus of 293T cells. 293T cells coexpressing RALY-BAP and BirA were fixed and stained with alexa-488 conjugated antistreptavidin (AV-488). Construct expressing the red fluorescence protein (RFP) was used as marker for cotransfection. Biotinylated RALY protein mainly accumulates within the nucleus as the endogenous demonstrating that biotinylation does not change RALY subcellular localization. In contrast, no signal of AV-488 is detected in cells expressing only RALY-BAP or BirA. UT, untransfected cells. Scale bar = 10 μ m.

based label-free quantification^{39,40} was performed using the ISOQuant software pipeline as described previously.³⁵

Bioinformatics and Statistical Analysis

Hierarchical clustering analysis was performed on the basis of absolute label-free protein quantification results provided by ISOQuant using dedicated R scripts in R2.14.0 execution environment.³⁵ Additional data processing was performed using DAVID (<http://david.abcc.ncifcrf.gov>).^{41,42} Subcellular localizations of RALY interacting proteins were predicted using WoLF-PSORT, TargetP and SubLoc Servers. Transmembrane helices were predicted using Phobius, TMHMM, TMPred and Scampi.^{38,43,44} For experiments stating *p*-values, a paired Student's *t* test was performed as described,³⁵ assuming significance at *p* < 0.05.

RESULTS

Our goal was to isolate RALY-containing RNPs from cellular extracts to decipher their molecular composition. The human RNA-binding protein RALY sequence contains a predicted RNA-recognition motif (RRM) at the N-terminal region

(Figure 1A and Figure S1A, Supporting Information). A sequence motif rich in glycine (GRR), whose function is still unclear, is present at the C-terminal region.⁴⁵ Moreover, two potential nuclear localization signals (NLS) were predicted by computer analysis, but their activity still remains uninvestigated in vivo. To gain information about the role of RALY in mammals, we determined its distribution within the cell by immunostaining. RALY showed a prominent nuclear accumulation, but it was excluded from the nucleoli as shown after the costaining with the nucleolar marker fibrillarin (Figure 1B). Similar localization pattern was observed in HeLa cells expressing RALY tagged with EGFP (data not shown). In addition, several discrete particles, typical staining for ribonucleoprotein (RNP) complexes, were also detected in the cytoplasm at the cell periphery (Figure 1C). An identical nuclear and cytoplasmic localization was observed in other cell types, including 293T cell lines, OVCAR3 and polarized cells such as oligodendrocytes (data not shown), demonstrating that the pattern observed was not cell-specific. To biotinylate RALY in vivo, 15 amino acids of the biotin acceptor peptide (BirA)

were added to the C-terminal region of RALY full length (Figure 1A). The resulting construct was then coexpressed in 293T cells together with BirA, a bacterial protein–biotin ligase.⁴⁶ We then proceeded to determine whether RALY was efficiently biotinylated *in vivo*. As expected, the antibody detected in untransfected cells a band at 37 kDa corresponding to the endogenously expressed RALY protein (Figure 1D, UT). Another band, shifted at the higher molecular weight, corresponding to biotinylated RALY (RALY-BAP), was detected by Western blot when cells expressed RALY-BAP together with BirA (Figure 1D). In contrast, no shifted band was observed when only RALY-BAP or BirA were expressed (Figure 1D). The localization of the endogenous RALY protein was also compared with the exogenously expressed BAP-tagged RALY. 293T cells coexpressing RALY-BAP together with the red fluorescent protein (RFP) were stained with the alexa 488-conjugated antistreptavidin antibody (AV-488) (Figure 1E). In untreated cells, a diffuse signal of AV-488 was observed (Figure 1E, UT). In contrast, a significant nuclear staining was detected only in those cells expressing RALY-BAP in the presence of BirA (Figure 1E, second row). As expected no nuclear staining was observed in cells expressing each single plasmid (Figure 1E, third and fourth row). All patterns analyzed were remarkably similar, indicating that the biotinylated protein behaves like the endogenous counterpart. Taken together, these data excluded the possibility that the position of the added tag influenced the intracellular localization of the resulting recombinant protein.

Having characterized the localization pattern of the endogenous as well as of the recombinant BAP-tagged RALY, we determined the protein composition of RALY-containing RNP complexes. The schematic outline of the purification procedure used in this study is shown in Figure S1B (Supporting Information). Cell extracts were prepared from 293T cells expressing RALY-BAP together with BirA. 293T cells expressing either RALY-BAP alone or BirA alone served as negative controls. The efficiency of biotinylation was verified by binding tagged RALY in crude cell extracts to streptavidin-coupled paramagnetic Dynabeads. Western blot analysis of the material eluted from the beads showed that tagged RALY protein was enriched in the pull-down (Figure 2A). In contrast, no RALY was detected in the pull-down in the absence of BirA (Figure 2A). The purified extracts were separated using SDS-PAGE and stained (Figure 2B). Silver staining of the gel loaded with purified RALY-BAP showed several bands that were not present in control cell lysates. To distinguish between RNA-dependent or -independent interactions, the cell lysate was incubated with RNase in order to disassemble RNP-complexes,⁴⁷ prior to incubation with streptavidin-beads. We observed an enrichment of specific bands after treatment with RNase compared to control treated lysate (Figure 2B). Taken together, these data show that RALY can be efficiently biotinylated and purified as RNP-complexes from cell extracts.

After the isolation of the pull-down samples treated either with or without RNase and control pull-downs from singly (either RALY-BAP, or BirA) transfected cells, eluted proteins were digested with trypsin. Tryptic peptides were separated by nanoUPLC directly coupled to a Synapt G2-S mass spectrometer operated in ion-mobility-enhanced data-independent acquisition mode. Overall, we were able to identify and quantify >220 proteins at <1% FDR (Table S1, Supporting Information). Table 1 shows the list of the 143 proteins that we found to be specifically associated with RALY (see also Figure 3A); of these, 113 were detectable only in pull-downs from

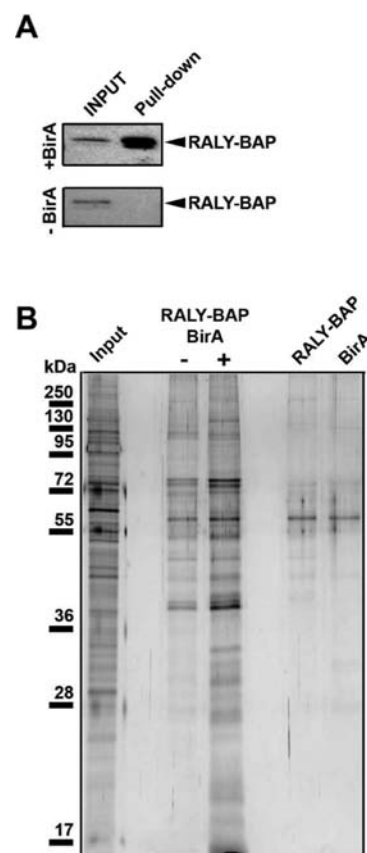


Figure 2. (A) Purification of RALY-tagged protein monitored by Western blot. 293T cells coexpressing RALY-BAP and BirA were washed and treated as described in Materials and Methods. As shown in the upper panel, RALY can be efficiently purified and enriched in the eluate. The Western blot was incubated with the HRP-conjugated antistreptavidin antibody. The lower panel shows that no purified RALY-BAP is detected in the flow through in the absence of BirA expression. Since no biotinylation of recombinant RALY occurs in the absence of BirA, the Western blot was decorated with the anti-RALY antibody. (B) Preparative purification of RALY from 293 T cell extract. The silver-stained 12% SDS-PAGE shows that the protein eluates from 293T cells expressing either RALY-BAP together with BirA, RALY-BAP or BirA. Cell lysate was prepared as described in Materials and Methods and incubated with (+) or without (–) RNase before the purification with streptavidin-coated beads (see also Figure S1B, Supporting Information). Input represents 10% of the loaded whole cells extract used for the pull-down experiments.

double-transfected cells, and another 30 proteins were found to be at least 2-fold more abundant compared to controls. The high proportion of proteins detected only in the pull-down samples confirmed the high specificity of the iBioPQ approach. Additionally, using TOP3-based absolute quantification, we determined the molar ratios of highest abundant interactors (Figure 3C). The most abundant interactors were HNRH1, MATR3 and HNRPF, which were present at approximately equimolar amounts.

Among identified putative RALY-interacting proteins, we confirmed the presence of NONO that has been recently identified as an interactor of YB1-containing complex together with RALY.¹⁷ In addition, some members of the hnRNP family such as hnRNP C1/2, hnRNP F, hnRNP K, hnRNP L, hnRNP M and hnRNP U were also identified. The biological roles of these molecules, which exert a plethora of roles in RNA metabolism, have been covered by several excellent re-

Table 1. Identification of RALY Binding Proteins Identified by iBioPQ^a

UniProt							
accession	ID	gene name	description	max score	reported peptides		RNase treatment
P62258	1433E	YWHAE	14-3-3 protein epsilon	2128.87	5		
Q9UKV3	ACINU	ACIN1	Apoptotic chromatin condensation inducer in the nucleus	1653.10	11		++
P63261	ACTG	ACTG1	Actin cytoplasmic 2	29066.54	13		
P05141	ADT2	SLC25A5	ADP ATP translocase 2	2064.63	4		
P25705	ATPA	ATPSA1	ATP synthase subunit alpha mitochondrial	1197.64	5		
Q9NYF8	BCLF1	BCLAF1	Bcl 2 associated transcription factor 1	507.21	3		
Q07021	C1QBP	C1QBP	Complement component 1 Q subcomponent binding protein mitochondrial	8074.07	5		++
P10809	CH60	HSPD1	60 kDa heat shock protein mitochondrial	1350.57	5		
Q9Y224	CN166	C14orf166	UPF0568 protein C14orf166	3827.05	4		++
Q92499	DDX1	DDX1	ATP dependent RNA helicase DDX1	5459.53	15		++
Q92841	DDX17	DDX17	Probable ATP dependent RNA helicase DDX17	5711.10	12		
O00571	DDX3X	DDX3X	ATP dependent RNA helicase DDX3X	4329.04	13		++
P17844	DDX5	DDX5	Probable ATP dependent RNA helicase DDX5	6412.09	12		++
Q9BQ39	DDX50	DDX50	ATP dependent RNA helicase DDX50	679.87	5		
Q7L2E3	DHX30	DHX30	Putative ATP dependent RNA helicase DHX30	5046.24	23		++
Q08211	DHX9	DHX9	ATP dependent RNA helicase A	8697.80	30		++
O60832	DKC1	DKC1	H ACA ribonucleoprotein complex subunit 4	2895.81	6		++
P49411	EFTU	TUFM	Elongation factor Tu mitochondrial	2949.42	5		++
Q15717	ELAV1	ELAVL1	ELAV like protein 1	785.05	3		--
P84090	ERH	ERH	Enhancer of rudimentary homologue	14686.37	3		
Q06787	FMR1	FMR1	Fragile X mental retardation protein 1	4229.49	7		++
P35637	FUS	FUS	RNA binding protein FUS	4455.03	3		++
P51114	FXR1	FXR1	Fragile X mental retardation syndrome related protein 1	2484.20	7		++
P51116	FXR2	FXR2	Fragile X mental retardation syndrome related protein 2	6090.89	12		++
P38646	GRP75	HSPA9	Stress 70 protein mitochondrial	3703.39	10		
Q9BQ67	GRWD1	GRWD1	Glutamate rich WD repeat containing protein 1	915.48	2		++
Q92522	H1X	H1FX	Histone H1x	10130.50	3		++
O60812	HNRCL	HNRNPCL1	Heterogeneous nuclear ribonucleoprotein C like 1	21886.77	12		++
P31943	HNRH1	HNRNPH1	Heterogeneous nuclear ribonucleoprotein H	17205.07	12		
P55795	HNRH2	HNRNPH2	Heterogeneous nuclear ribonucleoprotein H2	6796.38	7		
Q1KMD3	HNRL2	HNRNPUL2	Heterogeneous nuclear ribonucleoprotein U like protein 2	267.02	2		
P07910	HNRPC	HNRNPC	Heterogeneous nuclear ribonucleoproteins C1 C2	35024.63	21		
Q14103	HNRPD	HNRNPD	Heterogeneous nuclear ribonucleoprotein D0	1608.73	3		
P52597	HNRPF	HNRNPF	Heterogeneous nuclear ribonucleoprotein F	10977.72	6		
P61978	HNRPK	HNRNPK	Heterogeneous nuclear ribonucleoprotein K	5036.54	8		
P52272	HNRPM	HNRNPM	Heterogeneous nuclear ribonucleoprotein M	13139.34	28		
O43390	HNRPR	HNRNPR	Heterogeneous nuclear ribonucleoprotein R	1554.47	4		--
Q00839	HNRPU	HNRNPU	Heterogeneous nuclear ribonucleoprotein U	2608.45	9		--
P08107	HSP71	HSPA1A	Heat shock 70 kDa protein 1A 1B	9345.12	16		
P11142	HSP7C	HSPA8	Heat shock cognate 71 kDa protein	8124.75	14		
Q9NZI8	IF2B1	IGF2BP1	Insulin like growth factor 2 mRNA binding protein 1	1481.40	4		--
P38919	IF4A3	EIF4A3	Eukaryotic initiation factor 4A III	5958.01	9		
Q12905	ILF2	ILF2	Interleukin enhancer binding factor 2	1891.69	6		
Q12906	ILF3	ILF3	Interleukin enhancer binding factor 3	984.24	10		
P43243	MATR3	MATR3	Matrin 3	4921.41	11		--
Q9HCC0	MCCB	MCCC2	Methylcrotonoyl CoA carboxylase beta chain mitochondrial	29783.84	20		--
P61326	MGN	MAGOH	Protein mago nashi homologue	4326.43	2		
P07197	NFM	NEFM	Neurofilament medium polypeptide	1185.35	4		--
P55769	NH2L1	NHP2L1	NHP2 like protein 1	4685.52	2		++
Q9NX24	NHP2	NHP2	H ACA ribonucleoprotein complex subunit 2	9793.06	3		++
Q15233	NONO	NONO	Non-POU domain containing octamer binding protein	1258.06	3		
P55209	NP1L1	NAP1L1	Nucleosome assembly protein 1 like 1	2623.78	2		++
P06748	NPM	NPM1	Nucleophosmin	21390.75	9		++
P11940	PABP1	PABPC1	Polyadenylate binding protein 1	3219.85	9		--
Q13310	PABP4	PABPC4	Polyadenylate binding protein 4	2380.50	7		--
P05166	PCCB	PCCB	Propionyl CoA carboxylase beta chain mitochondrial	20069.40	19		--
Q96HS1	PGAM5	PGAM5	Serine threonine protein phosphatase PGAM5 mitochondrial	1921.23	4		
Q9UMS4	PRP19	PRPF19	Pre mRNA processing factor 19	1847.87	6		

Table 1. continued

UniProt							
accession	ID	gene name	description	max score	reported peptides		RNase treatment
Q32P51	RA1L2	HNRNPA1L2	Heterogeneous nuclear ribonucleoprotein A1 like 2	1509.86	2		++
Q9UKM9	RALY	RALY	RNA binding protein Raly	11463.77	14		
Q96PK6	RBM14	RBM14	RNA binding protein 14	604.41	3		
Q14498	RBM39	RBM39	RNA binding protein 39	1360.36	2		
Q9Y5S9	RBM8A	RBM8A	RNA binding protein 8A	6745.83	2		
Q14257	RCN2	RCN2	Reticulocalbin 2	8969.04	7		++
P27635	RL10	RPL10	60S ribosomal protein L10	3048.30	4		++
P62913	RL11	RPL11	60S ribosomal protein L11	21121.41	5		++
P30050	RL12	RPL12	60S ribosomal protein L12	22004.44	5		++
P40429	RL13A	RPL13A	60S ribosomal protein L13a	11425.01	5		++
P50914	RL14	RPL14	60S ribosomal protein L14	14799.98	3		++
P61313	RL15	RPL15	60S ribosomal protein L15	8458.17	4		++
P18621	RL17	RPL17	60S ribosomal protein L17	15467.44	5		++
Q07020	RL18	RPL18	60S ribosomal protein L18	20979.24	5		++
Q02543	RL18A	RPL18A	60S ribosomal protein L18a	5997.83	2		++
P84098	RL19	RPL19	60S ribosomal protein L19	17165.41	3		++
O76021	RL1D1	RSL1D1	Ribosomal L1 domain containing protein 1	2315.82	7		++
P35268	RL22	RPL22	60S ribosomal protein L22	10237.77	2		++
P62829	RL23	RPL23	60S ribosomal protein L23	20098.35	6		++
P62750	RL23A	RPL23A	60S ribosomal protein L23a	12431.37	5		++
P83731	RL24	RPL24	60S ribosomal protein L24	9559.97	4		++
P61353	RL27	RPL27	60S ribosomal protein L27	9041.97	4		++
P46776	RL27A	RPL27A	60S ribosomal protein L27a	13679.50	4		++
P46779	RL28	RPL28	60S ribosomal protein L28	10318.82	5		++
P47914	RL29	RPL29	60S ribosomal protein L29	10583.58	2		++
P39023	RL3	RPL3	60S ribosomal protein L3	4713.76	9		++
P62888	RL30	RPL30	60S ribosomal protein L30	30626.38	6		++
P62899	RL31	RPL31	60S ribosomal protein L31	17685.82	4		++
P62910	RL32	RPL32	60S ribosomal protein L32	22785.35	5		++
P49207	RL34	RPL34	60S ribosomal protein L34	11664.61	4		++
P42766	RL35	RPL35	60S ribosomal protein L35	5370.88	2		++
Q9Y3U8	RL36	RPL36	60S ribosomal protein L36	15226.67	3		++
P83881	RL36A	RPL36A	60S ribosomal protein L36a	5518.44	2		++
P46777	RL5	RPL5	60S ribosomal protein L5	16832.74	12		++
Q02878	RL6	RPL6	60S ribosomal protein L6	13973.62	10		++
P18124	RL7	RPL7	60S ribosomal protein L7	13322.13	9		++
P62424	RL7A	RPL7A	60S ribosomal protein L7a	17385.37	9		++
P62917	RL8	RPL8	60S ribosomal protein L8	9561.39	5		++
P05388	RLA0	RPLP0	60S acidic ribosomal protein P0	47057.78	12		++
P05386	RLA1	RPLP1	60S acidic ribosomal protein P1	71871.37	2		++
Q96E39	RMXL1	RBMXL1	RNA binding motif protein X linked like 1	3873.01	2		
P22626	ROA2	HNRNPA2B1	Heterogeneous nuclear ribonucleoproteins A2 B1	916.63	3		
P51991	ROA3	HNRNPA3	Heterogeneous nuclear ribonucleoprotein A3	1465.80	4		
P62280	RS11	RPS11	40S ribosomal protein S11	4369.03	4		++
P62277	RS13	RPS13	40S ribosomal protein S13	10457.01	3		++
P62249	RS16	RPS16	40S ribosomal protein S16	4115.29	2		++
P62269	RS18	RPS18	40S ribosomal protein S18	11165.43	5		++
P39019	RS19	RPS19	40S ribosomal protein S19	17796.30	6		++
P15880	RS2	RPS2	40S ribosomal protein S2	6647.55	5		++
P62266	RS23	RPS23	40S ribosomal protein S23	7508.04	3		++
P62847	RS24	RPS24	40S ribosomal protein S24	23479.49	2		++
P62851	RS25	RPS25	40S ribosomal protein S25	7363.56	3		++
P62854	RS26	RPS26	40S ribosomal protein S26	20581.14	3		++
P23396	RS3	RPS3	40S ribosomal protein S3	6653.01	7		++
P61247	RS3A	RPS3A	40S ribosomal protein S3a	20345.70	13		++
P62753	RS6	RPS6	40S ribosomal protein S6	13377.20	5		++
P46781	RS9	RPS9	40S ribosomal protein S9	7676.78	6		
P08865	RSSA	RPSA	40S ribosomal protein SA	2139.39	2		++
P82650	RT22	MRPS22	28S ribosomal protein S22 mitochondrial	7739.10	8		++

Table 1. continued

UniProt							
accession	ID	gene name	description	max score	reported peptides	RNase treatment	
Q92552	RT27	MRPS27	28S ribosomal protein S27 mitochondrial	7870.53	8	++	
Q9Y310	RTCB	C22orf28	tRNA splicing ligase RtcB homologue	4433.22	9	++	
O00422	SAP18	SAP18	Histone deacetylase complex subunit SAP18	4780.17	2	++	
Q12874	SF3A3	SF3A3	Splicing factor 3A subunit 3	517.52	2	--	
Q13435	SF3B2	SF3B2	Splicing factor 3B subunit 2	634.29	3		
Q15393	SF3B3	SF3B3	Splicing factor 3B subunit 3	1355.61	8	--	
P23246	SFPQ	SFPQ	Splicing factor proline and glutamine rich	1780.61	4	++	
Q9UQ35	SRRM2	SRRM2	Serine arginine repetitive matrix protein 2	342.98	8		
O75494	SRS10	SRSF10	Serine arginine rich splicing factor 10	4308.84	3		
Q07955	SRSF1	SRSF1	Serine arginine rich splicing factor 1	6424.17	5		
Q01130	SRSF2	SRSF2	Serine arginine rich splicing factor 2	1564.12	3		
P84103	SRSF3	SRSF3	Serine arginine rich splicing factor 3	21695.02	5		
Q13247	SRSF6	SRSF6	Serine arginine rich splicing factor 6	2556.39	4		
Q16629	SRSF7	SRSF7	Serine arginine rich splicing factor 7	19836.63	6		
Q13242	SRSF9	SRSF9	Serine arginine rich splicing factor 9	2428.25	3		
Q04837	SSBP	SSBP1	Single stranded DNA binding protein mitochondrial	21125.56	5		
P68363	TBA1B	TUBA1B	Tubulin alpha 1B chain	8048.62	7	++	
P07437	TBB5	TUBB	Tubulin beta chain	5734.63	8	++	
Q9Y2W1	TR150	THRAP3	Thyroid hormone receptor associated protein 3	985.35	6		
Q13595	TRA2A	TRA2A	Transformer 2 protein homologue alpha	1780.67	4		
P62995	TRA2B	TRA2B	Transformer 2 protein homologue beta	12611.33	6	++	
P26368	U2AF2	U2AF2	Splicing factor U2AF 65 kDa subunit	3166.23	6	++	
Q15029	USS1	EFTUD2	116 kDa U5 small nuclear ribonucleoprotein component	554.99	7		
P08670	VIME	VIM	Vimentin	27065.79	30		
P67809	YBOX1	YBX1	Nuclease sensitive element binding protein 1	3634.61	2	--	
Q5BKZ1	ZN326	ZNF326	DBIRD complex subunit ZNF326	1592.55	3		

^aProteins listed were either detected specifically in pulldowns from doubly transfected cells or showed at least 2.8-fold enrichment compared to controls. The effect of RNase treatment on the relative amount of each protein is indicated; (++)/(--) indicates >2-fold effects. The Max Score refers to the maximum identification score provided by PLGS (ProteinLynx Global Server) across all technical and biological replicates for the respective protein.

views.^{3,48–50} Moreover, several ribosomal proteins were also enriched in RALY-purified protein complex (Figure 3A). To gain insight into the various functions of the identified proteins, we performed gene ontology (GO) term analysis using DAVID. Statistically significant over represented ontologies of RALY-interacting proteins were grouped into 26 categories, mostly involved in RNA metabolism, including mRNA, rRNA and ncRNA processing, RNA stability, transport and translational control (Figure 4). Some categories comprised factors involved in ribosomal assembly, rRNA stability and posttranscriptional regulation. We then analyzed any changes in the molecular composition of RALY-containing complex upon treatment with RNase. Altogether, we observed significantly increased association of 80 proteins with RALY after RNase treatment (Table 1, Figure 3C). Among these proteins, we found factors involved in noncoding RNA (ncRNA) and rRNA processes, ribosome biogenesis, translation and translation elongation (Table 1 and Figure 4, green bars). In contrast, only 13 proteins mainly involved in RNA stability and splicing were decreased after the same treatment, suggesting that RALY might act as a bridge to link other protein complexes bound to the same mRNA. (Table 1 and Figure 4, red bars). Finally, 50 proteins remained unchanged (i.e., observed change was less than 2-fold), suggesting that their interactions with RALY were not affected by the presence (or absence) of intact RNA (Table 1 and Figure 4, yellow bars).

Next, we confirmed specific interaction of selected identified candidate proteins with RALY by Western blot analysis:

Matrin3 (MAT3),⁵¹ PABP1, eIF4AIII,^{52–54} the human homologue of *Drosophila mago nashi* protein (Magoh),⁵⁵ the Y-box binding protein 1 (YB-1),⁵⁶ PRP19,^{57,58} ELAVL1,^{59,60} the ribosomal protein L7a, the histone H1 and the fragile X mental retardation protein (FMRP).^{61–63} Western blot analysis confirmed the interactions of RALY with PABP, ELAVL1 and MAT3. As predicted, the interactions were mediated by an intact RNA (Figure 5A). Low but detectable amounts of Magoh protein and PRP19 were also detected in RALY pulldown, and their associations remained unchanged after treatment with RNase. In contrast, the disassembly of the RNP complexes by RNase increases the association of RALY with FMRP, eIF4AIII and hnRNP C, respectively (Figure 5A). To our surprise, we did not observe any pulldown of YB-1 with RALY as recently described by another group.¹⁷ Moreover, neither histone H1 nor RL7a were detected in RALY pulldown. To demonstrate the specificity of the observed interactions, two proteins not identified by mass spectrometry, namely the amyloid beta precursor protein (APP) and beta tubulin, were used as negative controls. In this case, no copurification of beta tubulin and APP proteins with RALY were observed (Figure 5B). Some proteins associated with RALY identified by iBioPQ, for example, the histone H1, hnRNP C and PRP19, are known to interact either directly or indirectly also with the DNA. To determine whether DNA could mediate the interactions of RALY with these molecules, cell lysates were treated with DNaseI before purification (Figure 5C). As Figure 5C shows,

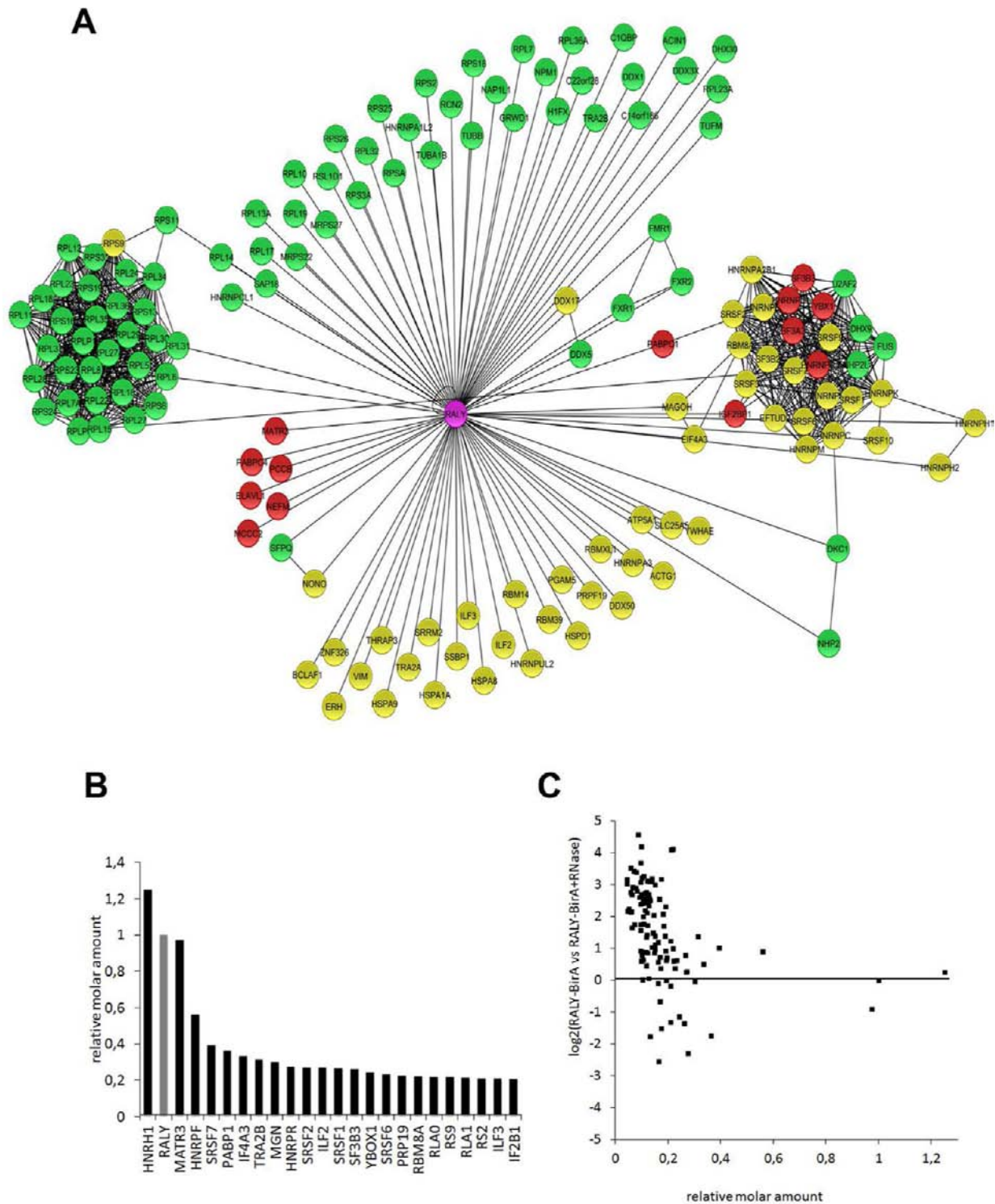


Figure 3. (A) Schematic network of RALY-interacting proteins identified by iBioPQ using Cytoscape program. Proteins that decrease or increase in RALY pull-down after RNase treatment are indicated in red and green colors, respectively. Black lines represent the interactions between RALY and its associated partners. RALY was linked with only a few proteins belonging to the major group of interactors. Proteins that remain unchanged after RNase treatment are depicted in yellow. The relationships among the different proteins were determined by using the String program (<http://string-db.org/>) with high confidence (score 0.7). (B) Relative molar amounts (normalized to RALY) of highest abundance interacting proteins as quantified using the TOP3 approach. (C) Quantitative analysis of the effects of RNase treatment on interacting proteins. The logarithmic change in relative amounts induced by RNase treatment was plotted vs the relative molar amount of the respective protein.

the treatment did not affect their association with RALY, demonstrating that the interaction does not require DNA.

Having verified the interaction of RALY with selected partners identified by mass spectrometry, we determined

whether our findings were consistent with their subcellular localization in 293T cells. We have established that RALY is mainly nuclear with a discrete cytoplasmic distribution. As expected, RALY showed an almost identical distribution pattern

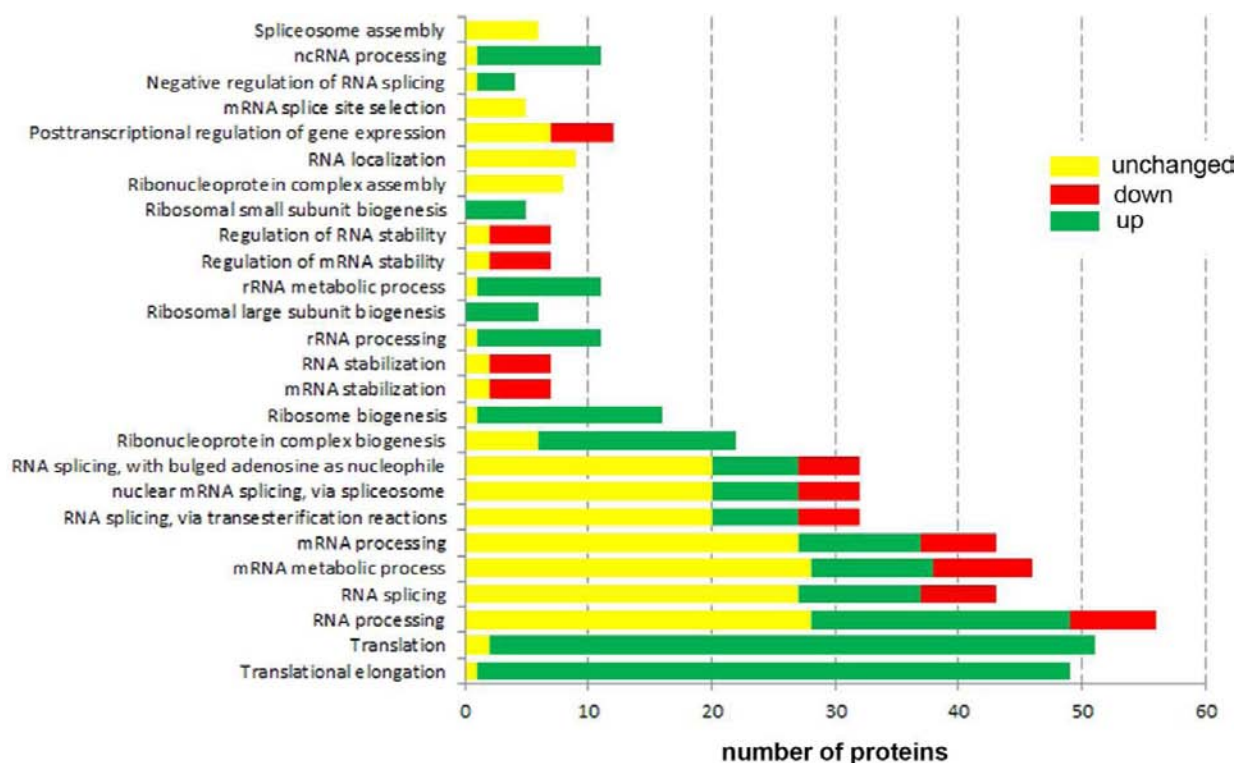


Figure 4. Functional annotation of RALY-associated proteins identified using analysis of GO term enrichment of the “biological process” category by DAVID. GO terms ranked according to the number of counts are plotted. All associations are significant ($p < 0.01$ after Bonferroni correction). Each bar represents the number of RALY’s interactors involved in 26 different biological processes. The amount of proteins that decrease, increase, or remain unchanged (i.e., display less than 2-fold change) in RALY pull-down after RNase treatment is depicted as in Figure 3A.

with hnRNP-C and ELAVL1 in the nuclear compartment (Figure 6A). The elongation initiation factor eIF4AIII is part of the exon-junction-complex (EJC),⁶⁴ but also component of the nonsense-mediated mRNA decay (NMD) machinery, was also identified in RALY pull-down upon treatment with RNase. As previously described, eIF4AIII was detected in the nucleoplasm and in the nuclear speckles, subnuclear domains containing pre-mRNA processing factors and noncoding RNAs that are involved in multiple steps of gene expression, including transcription, pre-mRNA processing and mRNA transport.^{53,65,66} Although RALY is not particularly enriched in the nuclear speckles, a colocalization with eIF4AIII was observed in the nucleoplasm (Figure 6A). PRP19 belongs to a complex that has a well-established and conserved function in mRNA splicing.⁶⁷ As for eIF4AIII, PRP19 localized to nucleoplasm and to dot-like structures that resemble nuclear speckles. RALY colocalization within the cell nucleus is similarly observed, although its signal is more diffuse throughout the nucleoplasm (Figure 6A). We also observed colocalization of RALY with MATR3. MATR3 was found both in the cytoplasm and in the nucleus as part of the nuclear matrix, excluding the nucleoli (Figure 6A). PABP showed a predominant cytoplasmic localization, and the immunostaining analysis did not reveal a significant colocalization with RALY in the nuclear compartment. However, subset of PABP particles showed colocalization with RALY in the cytoplasm at higher exposure (Figure 6B). Since PABP resides in the nuclear compartment, we cannot exclude that RALY might transiently interact with PABP also in this compartment. Taken together, these results show that RALY is in the same complex with the above-mentioned proteins, *in vitro* as well as *in vivo*.

In contrast to RALY, most hnRNPs contain repeats of Arg-Gly-Gly tripeptides domain and/or additional glycine-rich or proline-rich domains that seem to promote protein–protein interactions.^{3,68} We asked whether the peculiar glycine-rich domain (GRR) that RALY harbors at the C-terminal region was required for the interactions with the newly identified interactors (Figures S1A and S2B, Supporting Information). Thus, we performed pull down using extracts from cells that expressed RALY-BAP lacking the GRR (RALY-ΔGRR). We first determined the subcellular localization of RALY-ΔGRR by tagging the deleted protein with EGFP. The deleted form was not degraded when exogenously expressed by the cells. As for the full length, RALY lacking the glycine rich region localized in the nucleus but not in the nucleoli (Figure 6C). Moreover, RALY-ΔGRR still retained its RNA-binding activity (data not shown). These results demonstrate that the GRR domain is not necessary to target RALY to the nuclear compartment. To determine whether the GRR domain could modulate protein–protein interactions, 293T cells were transfected with the plasmid expressing BAP-tagged RALY-ΔGRR with or without BirA. Cell lysates were then treated with RNase or untreated, and the purified extracts were analyzed by Western blot (Figure 6D). The majority of the RNA-mediated interactions were unaffected by the absence of the GRR domain. Proteins such as PABP as well as MATR3 were copurified, and their interactions with RALY were still sensitive to RNase treatment, demonstrating that the lack of the GRR domain did not affect both RNA-dependent and independent interaction of RALY with newly identified interactors (Figure 6D, + RNase). We then tested for the presence of ELAVL1. Interestingly, ELAVL1 was not copurified with RALY-ΔGRR, suggesting that the GRR

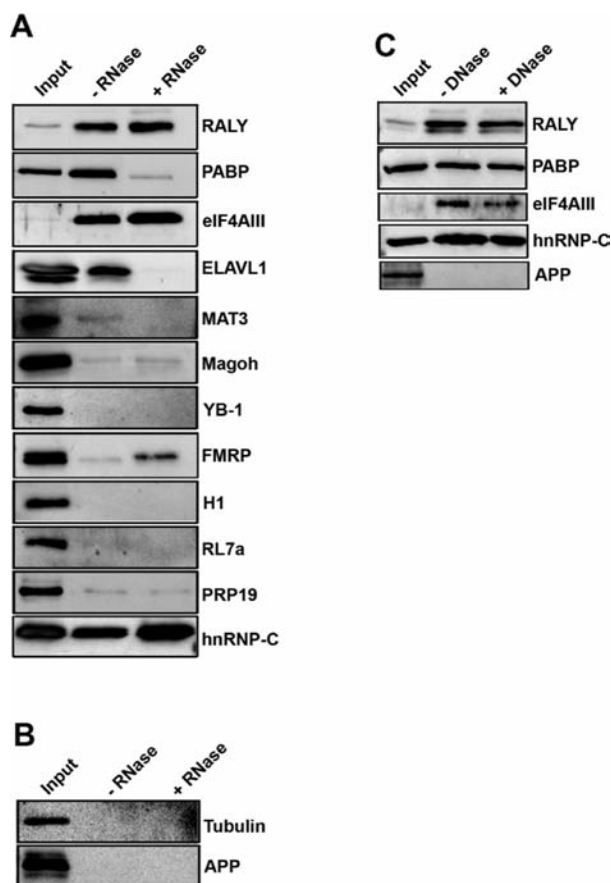


Figure 5. Pull-down of selected proteins with RALY. (A) Human 293T cells were transfected with plasmids expressing RALY-BAP and BirA. The purified eluates were analyzed by immunoblotting with the indicated antibodies. First lane: loaded whole cell extract (Input). Second lane represents the pull-down performed in the absence of RNase (-RNase). The third lane shows the pull-down performed in the presence of ribonucleases A (+RNase). Treatment with RNase enhanced the association of proteins such as eIF4AIII, Magoh, hnRNP-C/FMRP with RALY suggesting for protein–protein-based interactions. Interestingly, RALY can interact with itself in the absence of RNA. In contrast, RNA is required for the interaction of RALY with PABP, ELAVL1 and MAT3. No interaction is observed with RL7a and YB-1. (B) Western blot showing a control pull-down. Pull down of RALY does not involve either tubulin or APP. (C) Cell lysate was treated with DNase before purification, and the precipitated complexes were blotted with the indicated antibodies. In contrast to RNA, DNA does not mediate the interaction of RALY with the indicated proteins. APP was used as a negative control.

domain is required for the interaction with ELAVL1 even in the presence of RNA (Figure 6D).

DISCUSSION

The current work describes the identification of novel protein interactors of the RNA-binding protein RALY by an *in vivo* biotinylation pull-down-quantitative approach. The RNA-binding protein RALY, previously known as hnRNP C like-protein, contains a RNA-recognition motif similar to hnRNP C and two predicted NLS (Figure S2A, Supporting Information). Human RALY shares 87% identity with the mouse homologue, and the major differences are located within the C-terminal region (Figure S2A, Supporting Information). Moreover, RALY shares 43% amino acid identity with hnRNP C, and in contrast to hnRNP C and to other hnRNPs, RALY contains a peculiar

domain composed by a long stretch of glycine repeats (GRR) (Figure S2B, Supporting Information). The functional role of the GRR domain is unclear. Shorter glycine-rich repeats present in hnRNP A2 and hnRNP H/F seem to mediate their general intracellular trafficking.^{69,70} When expressed in mammalian cell lines, however, the intracellular localization of GFP-tagged RALY-ΔGRR was unchanged, and the protein still accumulated within the nucleus but not in the nucleoli. Although the subcellular localization as well as the RNA-binding activity of RALY was not altered by the absence of the GRR domain, the dynamics might be impaired. Could the GRR domain mediate protein–protein interactions? Pull-downs performed using RALY-ΔGRR assessed that the glycine-rich repeats is not required for the protein–protein interactions of RALY with some of the newly identified interactors (Figure 6D). However, the RNA-dependent interaction of ELAVL1 with RALY-ΔGRR was abolished, suggesting that the GRR domain might promote the recruitment of ELAVL1 and RALY to the RNA.

RALY has been found in complexes with molecules involved in RNA metabolism, but its biological role in the mammalian cells has not been thoroughly evaluated. In human, both RALY mRNA and protein are detected in several tissues,⁷¹ including the nervous system, kidney, liver, skeletal muscle, lung and pancreas. Interestingly, RALY mRNA is upregulated in many tumor tissues, even if associated functional implications are currently unknown.^{17,72} Although the modulation of RALY expression has been observed in different tumors, the role of RALY in tumorigenesis is a matter of ongoing investigation. While few interaction partners of RALY have been already described, a complete picture of the RALY interactome is lacking as no quantitative proteomic analysis of RALY RNP-complexes have been published so far. We isolated RALY complexes from cell cultures in order to identify possible molecular pathways in which RALY could be involved and gain information regarding its functions. Unfortunately, any attempt to immunoprecipitate RALY using various antibodies was unsuccessful or not efficient (data not shown). One explanation might rely on the observation that RALY, as many other RNA-binding proteins, is a constituent of large RNP-complexes, making it poorly accessible to the antibodies thereby hampering their immunoprecipitation under native conditions. To overcome this limitation, we expressed BAP-tagged RALY to purify RALY-containing complexes. Cotransfection with BirA leads to *in vivo* biotinylation of RALY, facilitating highly specific interaction of the *in vivo* biotinylated RALY with streptavidin-coated beads. A similar approach has been previously used to isolate mRNAs associated with the RNA-binding protein PABP.⁷³ Using cells transfected with untagged proteins and cells without BirA ligase, negative controls are readily available, rendering our method inexpensive, sensitive, and reliable. The strong interaction between biotin and streptavidin as well as the specificity of Bir(A) enzyme have several benefits: it increases the amount of purified protein, and in the same time, it decreases the number of unspecific interactors. Moreover, this approach minimizes the dissociation of weak interactions and thus maximizes the sensitivity of the approach and the yield of transient molecular interactors. These aspects are essential to reduce unspecifically bound proteins that would be falsely classified as potentially interacting proteins during subsequent mass spectrometric analysis. However, a major problem of mass spectrometric identification of potential interaction partners, even when using a high affinity pull-down and sensitive instrumentation, remains to distinguish interactors from

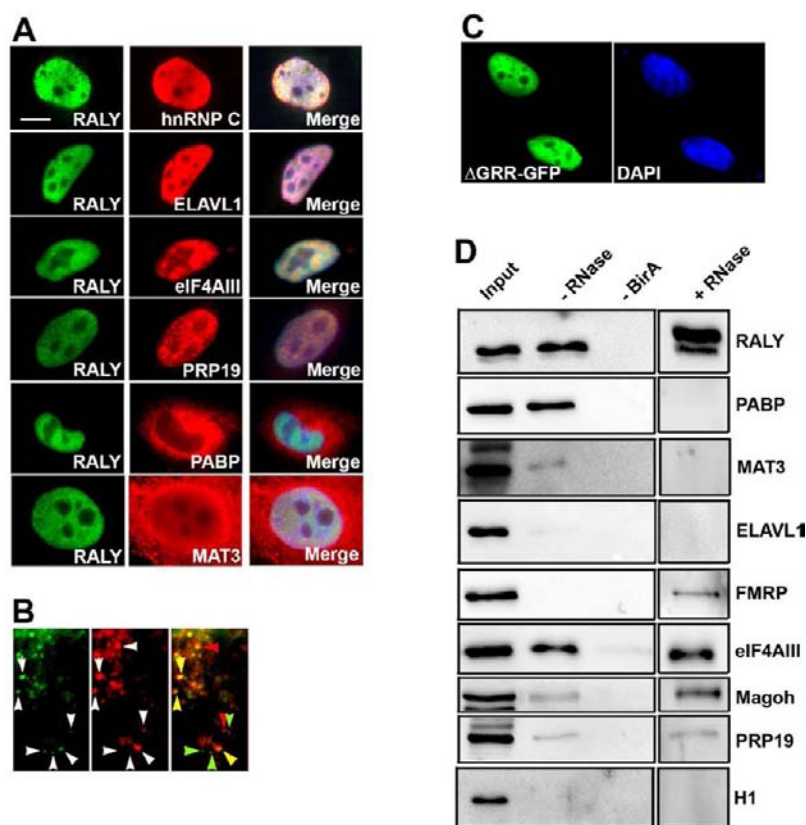


Figure 6. (A) Immunofluorescence microscopy of 293T cells showing colocalization of RALY (green) with the indicated proteins (in red). Scale bar = 5 μm . (B) High magnification image showing colocalization of RALY (green) and PABP (red) in the cytoplasm. Cells were fixed and stained as described in Materials and Methods. Particles colocalizing are indicated by yellow arrowheads. (C) Subcellular localization of deleted RALY in HeLa cells. EGFP-tagged RALY lacking the GRR domain still localizes in the nucleus except nucleoli. Scale bar = 5 μm . (D) GRR domain is not required for protein–protein interactions. Human 293T cells were transfected with plasmids expressing BAP-tagged RALY- Δ GRR with BirA. Control purification of 293T cells expressing BAP-tagged RALY- Δ GRR without BirA was done in parallel as a negative control. The purified eluates were separated on a 12% SDS-PAGE gel and analyzed by immunoblotting with the indicated antibodies.

proteins that bind unspecifically to the pull-down material. In the iBioPQ approach, parallel processing of pull-down and controls and subsequent label-free quantification by LC-MS^E allows to pinpoint potential interactors on the basis of their relative protein abundance ratio between pull-down and control samples, therefore increasing the specificity of interaction partner identification.

For mass spectrometric identification of interacting proteins, we applied an ion-mobility enhanced data-independent acquisition approach,^{36–38} which was previously used to quantify the composition of the myelin proteome.⁴⁴ In contrast to data-dependent acquisition (DDA), data-independent acquisition provides high technical reproducibility due to avoiding the stochastic nature of the peptide selection process. For example, in one previous study applying DDA, only 35–60% overlap of identified peptides was observed between technical replicates.⁷⁴ In contrast, we observed >90% overlap between both technical and biological replicates on protein level (see Figure S3, Supporting Information), thereby underlining the reproducibility of our approach. Additionally, no proteins were uniquely detected in control samples, which confirms the low unspecific background of our approach. Requiring candidates to be identified in both analyzed biological replicates provided additional stringency of the workflow.

Taken together, the iBioPQ approach allowed us to identify and quantify 143 novel molecular interactors of RALY. Among these, the protein NONO has been recently identified as an interactor of YB-1 containing complex together with RALY.¹⁷ Several hnRNPs were copurified with RALY, and among these were the hnRNP A1, C1/C2 and K. Although these factors play different roles in the metabolism, they can also interact with proteins involved in DNA damage response pathways.^{75,76} It will be interesting to determine whether RALY might change its intracellular localization upon DNA damage, supporting the emerging concept that RNA-binding proteins can be recruited to DNA damage sites and repair process with mechanisms that are still poorly investigated. Treatments with RNase allowed us to categorize RALY interactors into RNA-mediated interaction partners and direct (protein–protein) interactions. Interestingly, 80 identified interactors became enriched in RALY-containing complexes after RNase treatment. These results allow us to speculate cellular RNA to be a strong competitor for RALY, probably because of the high affinity of RALY for RNA. Thus, the interaction of RALY with additional proteins can be enhanced and/or stabilized upon depletion of RNA. Another hypothesis is that the lack of associated RNA changes the folding structure of RALY. These conformational changes might expose hidden domains of RALY allowing for additional interactions with other proteins. Many of the identified proteins are RNA-binding proteins (RBPs) known to be involved in

several processes of the RNA metabolism including rRNA and ncRNA metabolism, and RNP biogenesis. Most rewardingly, however, is the fact that a significant portion of the identified interactors is implicated in mRNA translational control. Our data suggest that RALY might have different functions in mRNA metabolism that need further investigations. Among the proteins identified in this study, eIF4AIII and FMRP showed a direct protein–protein interaction with RALY. The translation initiation factor eIF4AIII, Mago and Y14 are core components of the exon-junction-complex, a dynamic multiprotein complex that plays an essential role in nonsense mediated decay (NMD). The role of FMRP has been thoroughly investigated, especially in the nervous system. The loss of FMRP causes the Fragile X syndrome, the most common form of inherited intellectual disability.⁷⁷ In neurons, FMRP is a negative regulator of target mRNA translation important for neuronal development and synaptic function.^{78–80} FMRP is mainly found in the cytoplasm, but it shuttles into the nucleus where it binds to its cargo mRNAs.⁸¹ In neurons, both eIF4AIII and FMRP localize to dendrites in RNP complexes containing the double stranded RNA-binding protein Staufen and localized transcripts.⁸² Interestingly, eIF4AIII interacts with another member of the NMD machinery, MLN51/Barentsz (Btz), that is also a component of the dendritic mRNP.⁸³ For this reason, it would be interesting to determine whether RALY is also a component of the molecular machinery involved in mRNA subcellular localization in polarized cells such as neurons. Preliminary results confirm that RALY is present both in the cytoplasm and in distal processes of the oligodendroglial progenitor cell line Oli-neu^{84,85} (data not shown). It is tempting to speculate that RALY might remain associated with mRNAs during their transport and subsequent localization. It will be interesting to determine whether RALY can exert any role in local translational and/or RNA stability. Our data provide evidence that RALY interacts with proteins that exert pleiotropic roles in mRNA metabolism.

■ ASSOCIATED CONTENT

📄 Supporting Information

Figure S1. (A) ClustalW alignment of human RALY (Q9UKM9.1), *P. troglodytes* (XP_514591.2), *M. musculus* (Q64012.3), *R. norvegicus* (NP_001011958.1) and *D. rerio* (AAQ97838.1). Identical residues and conservative amino acid changes are marked by asterisks and dots, respectively. The domains schematically represented in Figure 1A are indicated by lines below the sequences: RNA-binding domain (yellow), NLS (red), and GRR (green). (B) Schematic representation of the procedure used to purify and characterize RALY interactors. Cells were transfected with two constructs expressing RALY tagged with the biotin acceptor peptide (BAP) and BirA, respectively. Additional cells were transfected with either RALY-BAP (Ctrl 1) or BirA (Ctrl 2) alone as controls. After 36 h, cells were washed and processed as described in Materials and Methods. Part of the lysate was directly incubated with streptavidin-coated magnetic beads, and the purified proteins were identified by mass spectrometry analysis. To identify proteins interacting with RALY in a RNA-independent way, the remaining of the lysate was treated with either RNase (or DNase in some cases) before purification. Figure S2. (A) Western blot showing the specificity of the purification. 293T cells were transfected with the construct expressing RALY-BAP. The cell lysates were then incubated with streptavidin-coated

magnetic beads. After several washing steps, the eluates were run on SDS-PAGE. Western blots were decorated with specific antibodies as indicated. No unspecific bond of the identified proteins is observed. The same results were obtained when 293T cells expressed only BirA in the absence of RALY-BAP. (B) ClustalW alignment of human RALY and human hnRNP C (NP_112604.2). Compared to RALY, hnRNP C protein does not contain the glycine rich region. Figure S3. Venn diagrams depicting (A) overlap between technical replicates, (B) overlap between biological replicates, and (C) overlap between pulldown and control samples. Venn Diagrams were constructed using the VENN web application. (<http://bioinfogp.cnb.csic.es/tools/venny/index.html>). Table S1. Complete listing of proteins identified in pulldowns and control samples. This material is available free of charge via the Internet at <http://pubs.acs.org>.

■ AUTHOR INFORMATION

Corresponding Author

*Phone: +39 0461 283819. Fax: +39 0461 283937. E-mail: macchi@science.unitn.it.

Author Contributions

#S. Tenzer and A. Moro contributed equally to this work.

Notes

The authors declare no competing financial interest.

■ ACKNOWLEDGMENTS

The plasmid to express Bir(A) was kindly provided by Dr. Oscar Burrone (ICGEB-International Centre for Genetic Engineering and Biotechnology, Trieste, Italy). We are grateful to Antonio Casini for technical advice. We thank Dr. Anna Cereseto for her comments on the manuscript and helpful discussion. This work was supported by the Forschungszentrum Immunologie (FZI) and the Naturwissenschaftlich-Medizinisches Forschungszentrum (NMFZ) of the Johannes-Gutenberg University Mainz (to S.T.), the University of Trento (Progetto Biotecnologie), CARITRO (Cassa di Risparmio di Trento e Rovereto) Foundation Grant (all to P.M.) and by the European Community's Seventh Framework Programme [FP7-2007-2013] under Grant Agreement No. HEALTH-F2-2011-256986 (to A.P. and P.M.).

■ REFERENCES

- (1) Krecic, A. M.; Swanson, M. S. hnRNP complexes: composition, structure, and function. *Curr. Opin. Cell Biol.* **1999**, *11* (3), 363–71.
- (2) Carpenter, B.; MacKay, C.; Alnabulsi, A.; MacKay, M.; Telfer, C.; Melvin, W. T.; Murray, G. I. The roles of heterogeneous nuclear ribonucleoproteins in tumour development and progression. *Biochim. Biophys. Acta* **2006**, *1765* (2), 85–100.
- (3) Han, S. P.; Tang, Y. H.; Smith, R. Functional diversity of the hnRNPs: past, present and perspectives. *Biochem. J.* **2010**, *430* (3), 379–92.
- (4) Ostareck-Lederer, A.; Ostareck, D. H. Control of mRNA translation and stability in haematopoietic cells: the function of hnRNPs K and E1/E2. *Biol. Cell* **2004**, *96* (6), 407–11.
- (5) Weighardt, F.; Biamonti, G.; Riva, S. The roles of heterogeneous nuclear ribonucleoproteins (hnRNP) in RNA metabolism. *Bioessays* **1996**, *18* (9), 747–56.
- (6) He, Y.; Smith, R. Nuclear functions of heterogeneous nuclear ribonucleoproteins A/B. *Cell. Mol. Life Sci.* **2009**, *66* (7), 1239–56.
- (7) Bailey-Serres, J.; Sorenson, R.; Juntawong, P. Getting the message across: cytoplasmic ribonucleoprotein complexes. *Trends Plant Sci.* **2009**, *14* (8), 443–53.

- (8) Kiebler, M. A.; Bassell, G. J. Neuronal RNA granules: movers and makers. *Neuron* **2006**, *51* (6), 685–90.
- (9) Percipalle, P.; Raju, C. S.; Fukuda, N. Actin-associated hnRNP proteins as transacting factors in the control of mRNA transport and localization. *RNA Biol.* **2009**, *6* (2), 171–4.
- (10) Giorgi, C.; Moore, M. J. The nuclear nurture and cytoplasmic nature of localized mRNPs. *Semin. Cell Dev. Biol.* **2007**, *18* (2), 186–93.
- (11) Hirokawa, N. mRNA transport in dendrites: RNA granules, motors, and tracks. *J. Neurosci.* **2006**, *26* (27), 7139–42.
- (12) Valverde, R.; Edwards, L.; Regan, L. Structure and function of KH domains. *FEBS J.* **2008**, *275* (11), 2712–26.
- (13) Rhodes, G. H.; Valbracht, J. R.; Nguyen, M. D.; Vaughan, J. H. The p542 gene encodes an autoantigen that cross-reacts with EBNA-1 of the Epstein Barr virus and which may be a heterogeneous nuclear ribonucleoprotein. *J. Autoimmun.* **1997**, *10* (5), 447–54.
- (14) Michaud, E. J.; Bultman, S. J.; Stubbs, L. J.; Woychik, R. P. The embryonic lethality of homozygous lethal yellow mice (Ay/Ay) is associated with the disruption of a novel RNA-binding protein. *Genes Dev.* **1993**, *7* (7A), 1203–13.
- (15) Duhl, D. M.; Stevens, M. E.; Vrieling, H.; Saxon, P. J.; Miller, M. W.; Epstein, C. J.; Barsh, G. S. Pleiotropic effects of the mouse lethal yellow (Ay) mutation explained by deletion of a maternally expressed gene and the simultaneous production of agouti fusion RNAs. *Development* **1994**, *120* (6), 1695–708.
- (16) Shav-Tal, Y.; Zipori, D. PSF and p54(nrb)/NonO—multifunctional nuclear proteins. *FEBS Lett.* **2002**, *531* (2), 109–14.
- (17) Tsoufack, S. P.; Garand, C.; Sereduk, C.; Chow, D.; Aziz, M.; Guay, D.; Yin, H. H.; Lebel, M. NONO and RALY proteins are required for YB-1 oxaliplatin induced resistance in colon adenocarcinoma cell lines. *Mol. Cancer* **2011**, *10*, 145.
- (18) Schitteck, B.; Psenner, K.; Sauer, B.; Meier, F.; Iftner, T.; Garbe, C. The increased expression of Y box-binding protein 1 in melanoma stimulates proliferation and tumor invasion, antagonizes apoptosis and enhances chemoresistance. *Int. J. Cancer* **2007**, *120* (10), 2110–8.
- (19) Ohga, T.; Uchiumi, T.; Makino, Y.; Koike, K.; Wada, M.; Kuwano, M.; Kohno, K. Direct involvement of the Y-box binding protein YB-1 in genotoxic stress-induced activation of the human multidrug resistance 1 gene. *J. Biol. Chem.* **1998**, *273* (11), 5997–6000.
- (20) Jurica, M. S.; Licklider, L. J.; Gygi, S. R.; Grigorieff, N.; Moore, M. J. Purification and characterization of native spliceosomes suitable for three-dimensional structural analysis. *RNA* **2002**, *8* (4), 426–39.
- (21) Sun, S.; Zhang, Z.; Fregoso, O.; Krainer, A. R. Mechanisms of activation and repression by the alternative splicing factors RBFOX1/2. *RNA* **2012**, *18* (2), 274–83.
- (22) Jin, Y.; Suzuki, H.; Maegawa, S.; Endo, H.; Sugano, S.; Hashimoto, K.; Yasuda, K.; Inoue, K. A vertebrate RNA-binding protein Fox-1 regulates tissue-specific splicing via the pentanucleotide GCAUG. *EMBO J.* **2003**, *22* (4), 905–12.
- (23) Underwood, J. G.; Boutz, P. L.; Dougherty, J. D.; Stoilov, P.; Black, D. L. Homologues of the *Caenorhabditis elegans* Fox-1 protein are neuronal splicing regulators in mammals. *Mol. Cell. Biol.* **2005**, *25* (22), 10005–16.
- (24) Pardo, M.; Lang, B.; Yu, L.; Prosser, H.; Bradley, A.; Babu, M. M.; Choudhary, J. An expanded Oct4 interaction network: implications for stem cell biology, development, and disease. *Cell Stem Cell* **2010**, *6* (4), 382–95.
- (25) Kelstrup, C. D.; Young, C.; Lavallee, R.; Nielsen, M. L.; Olsen, J. V. Optimized fast and sensitive acquisition methods for shotgun proteomics on a quadrupole Orbitrap mass spectrometer. *J. Proteome Res.* **2012**, *11* (6), 3487–97.
- (26) Paul, F. E.; Hosp, F.; Selbach, M. Analyzing protein–protein interactions by quantitative mass spectrometry. *Methods* **2011**, *54* (4), 387–95.
- (27) Pardo, M.; Choudhary, J. S. Assignment of protein interactions from affinity purification/mass spectrometry data. *J. Proteome Res.* **2012**, *11* (3), 1462–74.
- (28) Volkel, P.; Le Faou, P.; Angrand, P. O. Interaction proteomics: characterization of protein complexes using tandem affinity purification–mass spectrometry. *Biochem. Soc. Trans.* **2010**, *38* (4), 883–7.
- (29) Tate, S.; Larsen, B.; Bonner, R.; Gingras, A. C. Label-free quantitative proteomics trends for protein–protein interactions. *J. Proteomics* **2013**, *81*, 91–101.
- (30) Tirat, A.; Freuler, F.; Stettler, T.; Mayr, L. M.; Leder, L. Evaluation of two novel tag-based labelling technologies for site-specific modification of proteins. *Int. J. Biol. Macromol.* **2006**, *39* (1–3), 66–76.
- (31) de Boer, E.; Rodriguez, P.; Bonte, E.; Krijgsveld, J.; Katsantoni, E.; Heck, A.; Grosveld, F.; Strouboulis, J. Efficient biotinylation and single-step purification of tagged transcription factors in mammalian cells and transgenic mice. *Proc. Natl. Acad. Sci. U. S. A.* **2003**, *100* (13), 7480–5.
- (32) Rudra, D.; deRoos, P.; Chaudhry, A.; Niec, R. E.; Arvey, A.; Samstein, R. M.; Leslie, C.; Shaffer, S. A.; Goodlett, D. R.; Rudensky, A. Y. Transcription factor Foxp3 and its protein partners form a complex regulatory network. *Nat. Immunol.* **2012**, *13* (10), 1010–9.
- (33) Vidalino, L.; Monti, L.; Haase, A.; Moro, A.; Acquati, F.; Taramelli, R.; Macchi, P. Intracellular trafficking of RNASET2, a novel component of P-bodies. *Biol. Cell* **2012**, *104* (1), 13–21.
- (34) Wisniewski, J. R.; Zougman, A.; Nagaraj, N.; Mann, M. Universal sample preparation method for proteome analysis. *Nat. Methods* **2009**, *6* (5), 359–62.
- (35) Tenzer, S.; Docter, D.; Rosfa, S.; Wlodarski, A.; Kuharev, J.; Reikik, A.; Knauer, S. K.; Bantz, C.; Nawroth, T.; Bier, C.; Sirirattapan, J.; Mann, W.; Treuel, L.; Zellner, R.; Maskos, M.; Schild, H.; Stauber, R. H. Nanoparticle size is a critical physicochemical determinant of the human blood plasma corona: a comprehensive quantitative proteomic analysis. *ACS Nano* **2011**, *5* (9), 7155–67.
- (36) Geromanos, S. J.; Vissers, J. P.; Silva, J. C.; Dorschel, C. A.; Li, G. Z.; Gorenstein, M. V.; Bateman, R. H.; Langridge, J. I. The detection, correlation, and comparison of peptide precursor and product ions from data independent LC–MS with data dependant LC–MS/MS. *Proteomics* **2009**, *9* (6), 1683–95.
- (37) Silva, J. C.; Denny, R.; Dorschel, C. A.; Gorenstein, M.; Kass, I. J.; Li, G. Z.; McKenna, T.; Nold, M. J.; Richardson, K.; Young, P.; Geromanos, S. Quantitative proteomic analysis by accurate mass retention time pairs. *Anal. Chem.* **2005**, *77* (7), 2187–200.
- (38) Giles, K.; Pringle, S. D.; Worthington, K. R.; Little, D.; Wildgoose, J. L.; Bateman, R. H. Applications of a travelling wave-based radio-frequency-only stacked ring ion guide. *Rapid Commun. Mass Spectrom.* **2004**, *18* (20), 2401–14.
- (39) Silva, J. C.; Denny, R.; Dorschel, C.; Gorenstein, M. V.; Li, G. Z.; Richardson, K.; Wall, D.; Geromanos, S. J. Simultaneous qualitative and quantitative analysis of the *Escherichia coli* proteome: a sweet tale. *Mol. Cell. Proteomics* **2006**, *5* (4), 589–607.
- (40) Silva, J. C.; Gorenstein, M. V.; Li, G. Z.; Vissers, J. P.; Geromanos, S. J. Absolute quantification of proteins by LCMSE: a virtue of parallel MS acquisition. *Mol. Cell. Proteomics* **2006**, *5* (1), 144–56.
- (41) Huang da, W.; Sherman, B. T.; Tan, Q.; Collins, J. R.; Alvord, W. G.; Roayaei, J.; Stephens, R.; Baseler, M. W.; Lane, H. C.; Lempicki, R. A. The DAVID Gene Functional Classification Tool: a novel biological module-centric algorithm to functionally analyze large gene lists. *Genome Biol.* **2007**, *8* (9), R183.
- (42) Huang da, W.; Sherman, B. T.; Tan, Q.; Kir, J.; Liu, D.; Bryant, D.; Guo, Y.; Stephens, R.; Baseler, M. W.; Lane, H. C.; Lempicki, R. A. DAVID Bioinformatics Resources: expanded annotation database and novel algorithms to better extract biology from large gene lists. *Nucleic Acids Res.* **2007**, *35* (Web Server issue), W169–75.
- (43) Bradshaw, R. A.; Burlingame, A. L.; Carr, S.; Aebersold, R. Reporting protein identification data: the next generation of guidelines. *Mol. Cell. Proteomics* **2006**, *5* (5), 787–8.
- (44) Patzig, J.; Jahn, O.; Tenzer, S.; Wichert, S. P.; de Monasterio-Schrader, P.; Rosfa, S.; Kuharev, J.; Yan, K.; Bormuth, I.; Bremer, J.; Aguzzi, A.; Orfaniotou, F.; Hesse, D.; Schwab, M. H.; Mobius, W.; Nave, K. A.; Werner, H. B. Quantitative and integrative proteome

analysis of peripheral nerve myelin identifies novel myelin proteins and candidate neuropathy loci. *J. Neurosci.* **2011**, *31* (45), 16369–86.

(45) Pesiridis, G. S.; Lee, V. M.; Trojanowski, J. Q. Mutations in TDP-43 link glycine-rich domain functions to amyotrophic lateral sclerosis. *Hum. Mol. Genet.* **2009**, *18* (R2), R156–62.

(46) Howard, P. K.; Shaw, J.; Otsuka, A. J. Nucleotide sequence of the *birA* gene encoding the biotin operon repressor and biotin holoenzyme synthetase functions of *Escherichia coli*. *Gene* **1985**, *35* (3), 321–31.

(47) Mallardo, M.; Deitinghoff, A.; Muller, J.; Goetze, B.; Macchi, P.; Peters, C.; Kiebler, M. A. Isolation and characterization of Staufen-containing ribonucleoprotein particles from rat brain. *Proc. Natl. Acad. Sci. U. S. A.* **2003**, *100* (4), 2100–5.

(48) Chen, M.; Zhang, J.; Manley, J. L. Turning on a fuel switch of cancer: hnRNP proteins regulate alternative splicing of pyruvate kinase mRNA. *Cancer Res.* **2010**, *70* (22), 8977–80.

(49) Busch, A.; Hertel, K. J. Evolution of SR protein and hnRNP splicing regulatory factors. *Wiley Interdiscip. Rev.: RNA* **2012**, *3* (1), 1–12.

(50) Chaudhury, A.; Chander, P.; Howe, P. H. Heterogeneous nuclear ribonucleoproteins (hnRNPs) in cellular processes: Focus on hnRNP E1's multifunctional regulatory roles. *RNA* **2010**, *16* (8), 1449–62.

(51) Salton, M.; Elkon, R.; Borodina, T.; Davydov, A.; Yaspo, M. L.; Halperin, E.; Shiloh, Y. Matrin 3 binds and stabilizes mRNA. *PLoS One* **2011**, *6* (8), e23882.

(52) Alexandrov, A.; Colognori, D.; Steitz, J. A. Human eIF4AIII interacts with an eIF4G-like partner, NOM1, revealing an evolutionarily conserved function outside the exon junction complex. *Genes Dev.* **2011**, *25* (10), 1078–90.

(53) Palacios, I. M.; Gatfield, D.; St; Johnston, D.; Izaurralde, E. An eIF4AIII-containing complex required for mRNA localization and nonsense-mediated mRNA decay. *Nature* **2004**, *427* (6976), 753–7.

(54) Shibuya, T.; Tange, T. O.; Sonenberg, N.; Moore, M. J. eIF4AIII binds spliced mRNA in the exon junction complex and is essential for nonsense-mediated decay. *Nat. Struct. Mol. Biol.* **2004**, *11* (4), 346–51.

(55) Kataoka, N.; Diem, M. D.; Kim, V. N.; Yong, J.; Dreyfuss, G. Magoh, a human homolog of *Drosophila mago nashi* protein, is a component of the splicing-dependent exon-exon junction complex. *EMBO J.* **2001**, *20* (22), 6424–33.

(56) Kohno, K.; Izumi, H.; Uchiumi, T.; Ashizuka, M.; Kuwano, M. The pleiotropic functions of the Y-box-binding protein, YB-1. *Bioessays* **2003**, *25* (7), 691–8.

(57) Chanarat, S.; Seizl, M.; Strasser, K. The Prp19 complex is a novel transcription elongation factor required for TREX occupancy at transcribed genes. *Genes Dev.* **2011**, *25* (11), 1147–58.

(58) Sihm, C. R.; Cho, S. Y.; Lee, J. H.; Lee, T. R.; Kim, S. H. Mouse homologue of yeast Prp19 interacts with mouse SUG1, the regulatory subunit of 26S proteasome. *Biochem. Biophys. Res. Commun.* **2007**, *356* (1), 175–80.

(59) Chi, M. N.; Auriol, J.; Jegou, B.; Kontoyiannis, D. L.; Turner, J. M.; de Rooij, D. G.; Morello, D. The RNA-binding protein ELAVL1/HuR is essential for mouse spermatogenesis, acting both at meiotic and postmeiotic stages. *Mol. Biol. Cell* **2011**, *22* (16), 2875–85.

(60) Latorre, E.; Tebaldi, T.; Viero, G.; Sparta, A. M.; Quattrone, A.; Provenzani, A. Downregulation of HuR as a new mechanism of doxorubicin resistance in breast cancer cells. *Mol. Cancer* **2012**, *11*, 13.

(61) Till, S. M. The developmental roles of FMRP. *Biochem. Soc. Trans.* **2010**, *38* (2), 507–10.

(62) Zalfa, F.; Bagni, C. Another view of the role of FMRP in translational regulation. *Cell. Mol. Life Sci.* **2005**, *62* (2), 251–2.

(63) Feng, Y.; Absher, D.; Eberhart, D. E.; Brown, V.; Malter, H. E.; Warren, S. T. FMRP associates with polyribosomes as an mRNP, and the I304N mutation of severe fragile X syndrome abolishes this association. *Mol. Cell* **1997**, *1* (1), 109–18.

(64) Sauliere, J.; Murigneux, V.; Wang, Z.; Marquet, E.; Barbosa, L.; Le Tonqueze, O.; Audic, Y.; Paillard, L.; Roest Crolius, H.; Le Hir, H. CLIP-seq of eIF4AIII reveals transcriptome-wide mapping of the

human exon junction complex. *Nat. Struct. Mol. Biol.* **2012**, *19* (11), 1124–31.

(65) Chan, C. C.; Dostie, J.; Diem, M. D.; Feng, W.; Mann, M.; Rappaport, J.; Dreyfuss, G. eIF4A3 is a novel component of the exon junction complex. *RNA* **2004**, *10* (2), 200–9.

(66) Ferraiuolo, M. A.; Lee, C. S.; Ler, L. W.; Hsu, J. L.; Costa-Mattioli, M.; Luo, M. J.; Reed, R.; Sonenberg, N. A nuclear translation-like factor eIF4AIII is recruited to the mRNA during splicing and functions in nonsense-mediated decay. *Proc. Natl. Acad. Sci. U. S. A.* **2004**, *101* (12), 4118–23.

(67) Wahl, M. C.; Will, C. L.; Luhrmann, R. The spliceosome: design principles of a dynamic RNP machine. *Cell* **2009**, *136* (4), 701–18.

(68) Dreyfuss, G.; Matunis, M. J.; Pinol-Roma, S.; Burd, C. G. hnRNP proteins and the biogenesis of mRNA. *Annu. Rev. Biochem.* **1993**, *62*, 289–321.

(69) Sun, K. H.; Tang, S. J.; Wang, Y. S.; Lin, W. J.; You, R. I. Autoantibodies to dsDNA cross-react with the arginine-glycine-rich domain of heterogeneous nuclear ribonucleoprotein A2 (hnRNP A2) and promote methylation of hnRNP A2. *Rheumatology (Oxford, U. K.)* **2003**, *42* (1), 154–61.

(70) Van Dusen, C. M.; Yee, L.; McNally, L. M.; McNally, M. T. A glycine-rich domain of hnRNP H/F promotes nucleocytoplasmic shuttling and nuclear import through an interaction with transportin 1. *Mol. Cell. Biol.* **2010**, *30* (10), 2552–62.

(71) Khrebtukova, I.; Kuklin, A.; Woychik, R. P.; Michaud, E. J. Alternative processing of the human and mouse raly genes(1). *Biochim. Biophys. Acta* **1999**, *1447* (1), 107–12.

(72) Yang, X. Y.; Ren, C. P.; Wang, L.; Li, H.; Jiang, C. J.; Zhang, H. B.; Zhao, M.; Yao, K. T. Identification of differentially expressed genes in metastatic and non-metastatic nasopharyngeal carcinoma cells by suppression subtractive hybridization. *Cell Oncol.* **2005**, *27* (4), 215–23.

(73) Penalva, L. O.; Keene, J. D. Biotinylated tags for recovery and characterization of ribonucleoprotein complexes. *Biotechniques* **2004**, *37* (4), 604, 606, 608–10.

(74) Tabb, D. L.; Vega-Montoto, L.; Rudnick, P. A.; Variyath, A. M.; Ham, A. J.; Bunk, D. M.; Kilpatrick, L. E.; Billheimer, D. D.; Blackman, R. K.; Cardasis, H. L.; Carr, S. A.; Clauser, K. R.; Jaffe, J. D.; Kowalski, K. A.; Neubert, T. A.; Regnier, F. E.; Schilling, B.; Tegeler, T. J.; Wang, M.; Wang, P.; Whiteaker, J. R.; Zimmerman, L. J.; Fisher, S. J.; Gibson, B. W.; Kinsinger, C. R.; Mesri, M.; Rodriguez, H.; Stein, S. E.; Tempst, P.; Paulovich, A. G.; Liebler, D. C.; Spiegelman, C. Repeatability and reproducibility in proteomic identifications by liquid chromatography-tandem mass spectrometry. *J. Proteome Res.* **2010**, *9* (2), 761–76.

(75) Lee, S. W.; Lee, M. H.; Park, J. H.; Kang, S. H.; Yoo, H. M.; Ka, S. H.; Oh, Y. M.; Jeon, Y. J.; Chung, C. H. SUMOylation of hnRNP-K is required for p53-mediated cell-cycle arrest in response to DNA damage. *EMBO J.* **2012**, *31* (23), 4441–52.

(76) Haley, B.; Paunesku, T.; Protic, M.; Woloschak, G. E. Response of heterogeneous ribonuclear proteins (hnRNP) to ionising radiation and their involvement in DNA damage repair. *Int. J. Radiat. Biol.* **2009**, *85* (8), 643–55.

(77) De Rubeis, S.; Fernandez, E.; Buzzi, A.; Di Marino, D.; Bagni, C. Molecular and cellular aspects of mental retardation in the Fragile X syndrome: from gene mutation/s to spine dysmorphogenesis. *Adv. Exp. Med. Biol.* **2012**, *970*, 517–51.

(78) Liu-Yesucevitz, L.; Bassell, G. J.; Gitler, A. D.; Hart, A. C.; Klann, E.; Richter, J. D.; Warren, S. T.; Wolozin, B. Local RNA translation at the synapse and in disease. *J. Neurosci.* **2011**, *31* (45), 16086–93.

(79) Dahm, R.; Macchi, P. Human pathologies associated with defective RNA transport and localization in the nervous system. *Biol. Cell* **2007**, *99* (11), 649–61.

(80) Zalfa, F.; Giorgi, M.; Primerano, B.; Moro, A.; Di Penta, A.; Reis, S.; Oostra, B.; Bagni, C. The fragile X syndrome protein FMRP associates with BC1 RNA and regulates the translation of specific mRNAs at synapses. *Cell* **2003**, *112* (3), 317–27.

(81) Kim, M.; Bellini, M.; Ceman, S. Fragile X mental retardation protein FMRP binds mRNAs in the nucleus. *Mol. Cell. Biol.* **2009**, *29* (1), 214–28.

(82) Giorgi, C.; Yeo, G. W.; Stone, M. E.; Katz, D. B.; Burge, C.; Turrigiano, G.; Moore, M. J. The EJC factor eIF4AIII modulates synaptic strength and neuronal protein expression. *Cell* **2007**, *130* (1), 179–91.

(83) Macchi, P.; Kroening, S.; Palacios, I. M.; Baldassa, S.; Grunewald, B.; Ambrosino, C.; Goetze, B.; Lupas, A.; St; Johnston, D.; Kiebler, M. Barentsz, a new component of the Staufen-containing ribonucleoprotein particles in mammalian cells, interacts with Staufen in an RNA-dependent manner. *J. Neurosci.* **2003**, *23* (13), 5778–88.

(84) Jung, M.; Kramer, E.; Grzenkowski, M.; Tang, K.; Blakemore, W.; Aguzzi, A.; Khazaie, K.; Chlichia, K.; von Blankenfeld, G.; Kettenmann, H.; et al. Lines of murine oligodendroglial precursor cells immortalized by an activated neu tyrosine kinase show distinct degrees of interaction with axons in vitro and in vivo. *Eur. J. Neurosci.* **1995**, *7* (6), 1245–65.

(85) White, R.; Gonsior, C.; Kramer-Albers, E. M.; Stohr, N.; Huttelmaier, S.; Trotter, J. Activation of oligodendroglial Fyn kinase enhances translation of mRNAs transported in hnRNP A2-dependent RNA granules. *J. Cell Biol.* **2008**, *181* (4), 579–86.